ISSN 0972-5741

IGC Newsletter

INDIRA GANDHI CENTRE FOR ATOMIC RESEARCH

http://www.igcar.gov.in/newsletter/igc139.pdf

Volume 139, Issue 1, January 2024

Contents

New Year 2024 Message

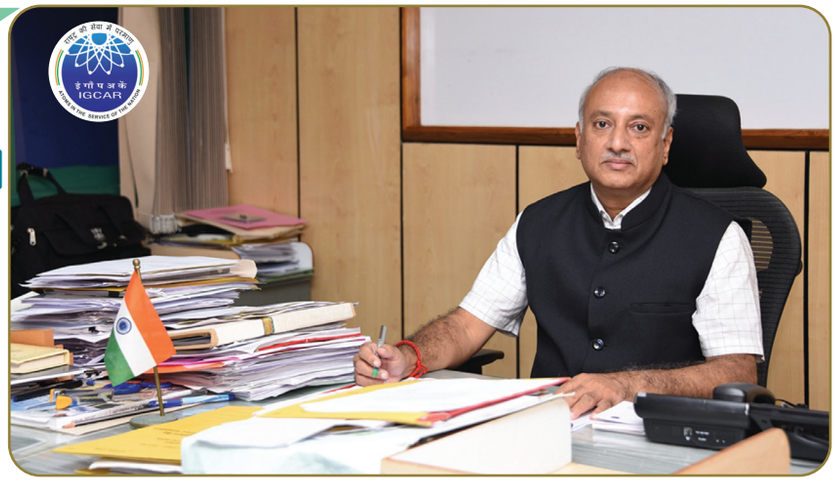

Dear Colleagues,

It is my pleasure to wish all colleagues of Indira Gandhi Centre for Atomic Research and General Services Organization and their near and dear ones a very joyous, healthy, blissful and prosperous New Year 2024.

As we enter into the coming New Year, it is time to rejoice on the achievements and retrospect on the challenges towards setting our goals in the coming years.

In the year 2023, the flagship of our Centre - Fast Breeder Test Reactor (FBTR) successfully completed 32 irradiation campaigns including three irradiation campaigns at 40 MWt since its first criticality in 1985. In 2023, 21.5 Million units of electricity was generated, which is equivalent to savings of 21,500 tones of CO_2 emission with a cumulative Effective Full Power Days (EFPD) of operation of 115 days. Testing of different composition of Pu/U/Zr metallic fuel is continuing, production of strontium isotope and revamping of many safety related systems has been completed. FBTR has been relicensed for operation up to June 28, 2028. The 233U based Kalpakkam Mini Reactor (KAMINI) continued to operate up to 30 kWt for neutron radiography of irradiated fuel pins, activation analysis of samples from AMD-Hyderabad, ASI,

National Forensic Sciences University, other institutions and testing of neutron detectors from M/s ECIL.

The Prototype Fast Breeder Reactor (PFBR) at BHAVINI is in an advanced stage of integrated commissioning and IGCAR continues to provide the required technical support. Many colleagues from various groups of IGCAR are working in synergy with BHAVINI team for the commissioning activities. Major activities like sodium performance testing of the integrated Failed Fuel Location Module (FFLM), the Independent Verification and Validation (IV&V) activities of 17 Real Time Computing (RTC) systems required for Main Vessel Sodium Filling, obtaining regulatory clearances, Support for completion of sodium filling in Main vessel, transfer arm modification works, and operation of primary sodium pumps have been successfully accomplished. Support has also been provided towards commissioning of shutdown systems, fuel handling systems, Primary and secondary sodium pumps, Eddy current flow meter, Annular Linear Induction pumps etc. in PFBR. Activities towards transfer of sodium to the upcoming Sodium Technology Complex (STC) are in full swing.

COmpact Reprocessing facility for Advanced fuels in Lead shielded cells (CORAL), facility has successfully completed its 65th campaign and is continuing to function normally well beyond its design intent. CORAL facility has been relicensed for operation by AERB for a further period of 5 years (up to 2028). Commissioning of Demonstration fast reactor Fuel Reprocessing Plant (DFRP), has reached an advanced stage after the successful completion of the cold run with natural uranium. Necessary responses to queries from AERB for hot commissioning are being addressed and the final approval is expected soon.

As part of metal fuel development activities, the metal fuel, U-Zr, about 200 slugs was produced through injection casting technique. Following electro-refining of uranium metal using pyro-process from a 10 kg facility, the heavy metal from cathode product was consolidated for its ingot production. The radioisotope, Y-90 was isolated from FR-HLLW by separating it out from Sr-90. The first batch of the product has been prepared for its qualification.

In our endeavour towards indigenous development of improved materials and processes, a new Ni-base super-alloy for use in boilers operating at high temperatures has been indigenously manufactured through a multi-organisation collaborative effort involving IGCAR, MIDHANI and NFC. PIE of high LHR operated Mark – I SA has been completed. A facility for studying the structural stability simultaneously at various pressures and temperatures by X-ray diffraction has been established at beam line of INDUS-2, RRCAT (Raja Ramanna Centre for Advanced Technology) through collaborative efforts of scientists from IGCAR & RRCAT units. Control system for 1.7 MV tandetron accelerator has been recently developed with in-house expertise and successfully tested.

Two technologies developed under “Atma Nirbhar Bharat” programmes of IGCAR have been successfully transferred to industry through the Incubation Centre. Two Indian patents have been granted. A collaborative incubation agreement is in place with an industry for completing development of IGCAR’s “Oil Level Measurement System” technology.

Continuing the commitment towards neighborhood community welfare, IGCAR facilitated a Memorandum of Agreement (MoA) between BARC (DAE) and Gram Panchayats of four neighbouring villages around Kalpakkam DAE Complex, Chengalpet District, Tamil Nadu; for setting-up of BARC developed desalination and membrane based RO water purification plant, ultra filtration-membrane based POU (Point-Of-Use) devices and water treatment plant which were installed at different places to benefit the local population.

As part of implementation of DAE Technologies of societal relevance, “Mobile Health – Wellness Program for the Rural Population” has been carried out in the rural areas in and around Chengalpet region, in collaboration with SRM Institute of Science and Technology and SRM Hospitals, Kattankulathur, Tamilnadu. DAE developed health care technologies like OncoDiagnoscope (RRCAT) for detecting oral cancer, Tubercular Scope (RRCAT) for detecting TB, Tele ECG (BARC) for monitoring activity of heart along with IR camera for breast cancer detection (IGCAR) in women are deployed in a mobile van. During May 2023, camps were conducted in the villages in and around Chengalpet, TN. More than 1400 villagers attended and benefited from this free medical camp. Free health camps are being planned by IGCAR in

collaboration with SRM University, AP Amaravati & AIIMS – Mangalagiri for benefitting people from surrounding villages.

Towards production of Sr-89 radiopharmaceutical from yttria, production of five batches has been successfully completed and radiochemical quality control has been established. Further activities, including scaling up of the process, Bio-distribution studies etc. are in progress. More than 600 numbers of radiation protection instruments from Hospitals, Nuclear Medicine Centres, Industry, and Research organizations apart from DAE institutions, have been calibrated at the NABL Accredited, Regional Calibration Facility (RCF) which has been augmented with a highly radioactive Co-60 source of 20Ci. The "Anu Awareness Yatra - 2023" with the theme of 'ATOMS IN THE SERVICE OF THE NATION' was organized by IGCAR, Kalpakkam in association with the National Council of Science Museum (NCSM), Ministry of Culture, Government of India, Vigyan Bharathi – Arivial Sangam, Tamil Nadu and Indian Association for Radiation Protection. This awareness program was organized in nodal institutions across 7 districts of Tamil Nadu & 3 districts of Kerala as part of 'Azadi Ka Amrit Mahotsav', to showcase the indigenous progress in Science and Technology, from July 24 to August 14, 2023. An exhibition displaying India's nuclear power programme and societal applications of technologies developed by DAE was also organised with more than 15,000 foot falls.

Towards human resources development, twenty nine young trained scientists and engineers (OCES-2022, 17th Batch) have successfully completed their orientation programme at BARC Training School at IGCAR and have been placed in various units of DAE. About 200 students have pursued project work and about 1200 students and faculty have visited the Centre in the last year. STIPAC and BITS Practice School programmes continue as in the previous years.

Engineering Services has made significant and unique contribution by way of repair/modification of critical components of PFBR. Among various infrastructures that were completed by CEG & ESG to support the R&D activities, a notable achievement is the commissioning of Tertiary water treatment plant of capacity 400 cu. m per day.

General Services Organization continues to efficiently maintain the residential and infrastructural buildings and maintaining the townships serene, green and clean. The Medical Group has provided good services to the CHSS beneficiaries and to the surrounding community. The Administration, Accounts and Auxiliary Departments of IGCAR and GSO have continued to provide commendable services guiding and supporting the execution of the programmes.

I take this opportunity to place our thanks to the principals, teachers and staff of Kendriya Vidayalayas Atomic Energy Central Schools within our township premises for providing holistic education to our wards. The performance of the students in board exams from all the five schools has been exemplary.

Towards the way forward in 2024, apart from the other R&D and regular activities at the various groups of IGCAR and GSO, our focus would continue to be providing support for the integrated commissioning activities of PFBR towards higher temperature operation after Main Vessel Sodium Filling, Completion of IV&V activities of balance RTC systems required for Initial Fuel Loading and subsequent First Approach to Criticality. The hot commissioning of DFRP and operation of DFRP with spent fuel from fast reactor, continuing to operate FBTR at 40 MWt for 90 EFPD, irradiation of advanced FBR structural materials, study the feasibility of producing hydrogen from FBTR super heated steam in collaboration with BARC, commissioning of 1 m fuel pin fabrication facility towards casting U-Pu-Zr metal fuel along with electro-refining facility, producing radioisotope P-32 through irradiation of $SrSO_4$ at FBTR and supply the first batch of radioisotope P-32 to BRIT; and dedication of Doppler Weather Radar Facility would be the milestones to complete in 2024.

I look forward to your support and co-operation in the coming year 2024!.

B. Venkatraman
Director, IGCAR & GSO

Editor's Desk

Dear Reader

Greetings

It is my pleasant privilege to forward the latest issue of IGC Newsletter (Volume 139, January 2024, Issue 1). I thank my team for their timely inputs, cooperation, and support in bringing out this issue.

The technical article of this issue "Radiocarbon Measurements in the Atmosphere" is by Dr. B.Arun and colleagues from RAMS, RESD, SQRMG, IGCAR.

Young Officer's Forum features an article on "Highly Efficient Post-Synthetically Modified UiO-66 MOF for the Extraction of Pd(II) from Aqueous Solutions: Experimental and Theoretical studies" by Shri Somnath Sengupta from FCHD, MCMFCG, IGCAR.

The article on "Large Area Monolayer MoS2: Enhanced Optical and Electronic Properties" by Shri Shri Choudhary Abinash Bhuyan from SSSD, MSG, IGCAR is categorised as this issue's Young Researcher article.

In the back cover, we have Lesser Goldenback bird very commonly found in both IGCAR campus and Kalpakkam township.

The Editorial Committee would like to thank all the contributors. We look forward to receiving constructive suggestions from readers towards improving the IGC Newsletter content.

We express our deepest gratitude to Director IGCAR for his keen interest and guidance.

Shri J. Rajan
With best wishes and regards
Chairman, Editorial Committee, IGC Newsletter and
Head, Scientific Information & Networking Division, IGCAR

Radiocarbon Measurements in the Atmosphere

Introduction

Radiocarbon (^{14}C) is a pure beta emitter with endpoint energy of 156 KeV. The half-life of ^{14}C is 5730±40 years. The existence of ^{14}C in atmospheric CO_2 is due to natural cosmogenic production, atmospheric nuclear weapon testing, and nuclear power plants. The released carbon-14 from the nuclear power plants is integrated into the natural carbon cycle in the environment and then into the food chain. Hence, monitoring carbon-14 in the vicinity of nuclear power plants is essential to observe any increase in natural background levels.

Quantification of ^{14}C concentration in the atmosphere is carried out in two steps using a liquid scintillation counter (LSC). In the first step, $^{14}CO_2$ in the atmosphere is absorbed in a suitable absorbing media. In the next step, the absorbed $^{14}CO_2$ in absorbing media is analyzed for ^{14}C concentration using a liquid scintillation counter.

Sampling of $^{14}CO_2$ in the atmosphere can be carried out using either active or passive sampling techniques. In the active sampling technique, air is pulled through a pump, and $^{14}CO_2$ present in the air is absorbed using a chemical trap. However, in the passive sampling method, $^{14}CO_2$ present in the air is absorbed using a chemical trap by spontaneous diffusion of $^{14}CO_2$ molecules. The advantage of the passive sampling technique is that the $^{14}CO_2$ in the atmosphere can be collected in any remote area without a power supply requirement. The advantage of active sampling is that it will provide a precise concentration of ^{14}C (Bq/m^3) in the air. In contrast, the passive sampling method will give relative values that are specific activity levels of ^{14}C (Bq/kg of carbon).

In this paper, optimization of the sampling period, absorption capacity of CO_2 in sodium hydroxide (NaOH) solution, recovery, and measurement of carbon-14 in the atmosphere by active and passive sampling technique is discussed.

Measurement methodology

The flow chart of sampling and measurement methodology for the carbon-14 was shown in Figure 1. In active and passive sampling techniques, CO_2 present in the atmosphere was absorbed using a sodium hydroxide solution. Absorbed CO_2 in NaOH was precipitated as barium carbonate ($BaCO_3$) by the addition of barium chloride ($BaCl_2$). The resulted $BaCO_3$ was dried after precipitation and then subjected to acid hydrolysis. The CO_2 released in acid hydrolysis was absorbed into Carbo-Sorb E/Permafluor (absorption mixture) and measured for carbon-14 activity levels using the LSC. The specific activity (A_s) of carbon-14 in the sample was calculated using eq-1.

$$A_S = \frac{(n_s - n_b) * 1000}{\varepsilon * m} \pm \frac{\sqrt{(n_s + n_b) * T} * 1000}{\varepsilon * m * T} \quad [1]$$

Where, As is the specific activity of the sample (Bq/(kg C)), n_s and n_b are the sample and background count rate, respectively, (counts per second, cps); T is counting time, ε is the counting efficiency (cps/Bq) of the LSC, m is the mass of carbon (g) absorbed in the absorber.

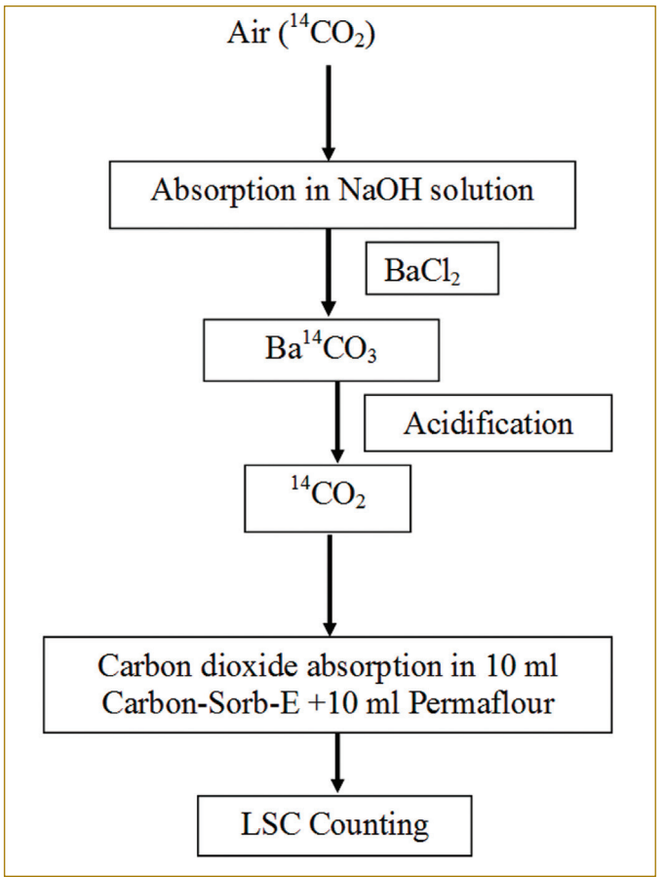

Figure 1: Flow Chart for sampling and measurement of Carbon-14 in the atmosphere

CO_2 absorption method

The CO_2 absorption method was used as a pre-treatment method for the measurement of ^{14}C. The experimental setup for CO_2 absorption method was shown in Figure 2. The barium carbonate precipitate obtained from the air sample was acidified using 100 ml of 2.5N hydrochloric acid (HCl). The released CO_2 gas was absorbed in a scintillation absorption mixture. The scintillation absorption mixture contains 10 ml of Carbo-Sorb E (3-methoxy propylamine, CS) and 10 ml of Permaflour Scintillator (PE) cocktail. The difference in the weight

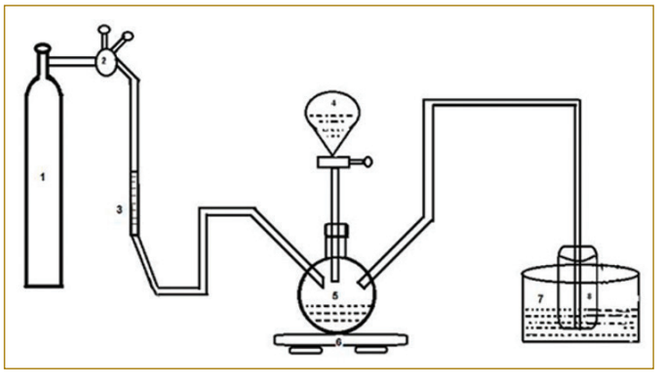

Figure 2: Experimental set up for carbon dioxide absorption method. 1. Nitrogen Cylinder, 2. Control valve, 3. Flow meter, 4. Dropping funnel, 5. Three neck 250ml flask, 6. Magnetic stirrer, 7. Ice-bath, 8. 20 mL measurement vial

of the 20 ml vial absorption mixture before and after CO_2 absorption indicates the amount of CO_2 absorbed. The scintillation absorption solution, after absorption of CO_2, was kept in the dark overnight to reduce the chemiluminescence counts before counting in the LSC.

Measurement of ^{14}C Using LSC

The specific activity of ^{14}C was measured using a Hidex Make 300SL LSC. The system contains three photomultiplier tubes (PMTs) to detect the scintillation light. The three PMTs were kept at 120^0 angles apart to cover isotropic geometry. The lead shielding (70 mm thick) was used to reduce the natural background counts. Additionally Sodium iodide doped with thallium (NaI (Tl)) based scintillation detector used as guard counter which was operated in anticoincidence counting mode to reduce the background counts. The sample measurements were carried out with coincidence counting mode in the time frame of 35 ns from the three PMTs. The triple-to-double coincidence ratio (TDCR) method was used to monitor and estimate the quench present in the samples. All the measurements of the standard, sample, and background were carried out in similar geometrical and chemical conditions. Low potassium (^{40}K) content borosilicate glass vials with 20 ml volume were used for the measurements. The counting time for the sample measurements was 200 minutes.

Minimum Detectable Activity (MDA)

The minimum detection limit (MDA) was calculated using the eq-2. The background measurements were carried out with a saturated scintillation absorption mixture of CS & PE with CO_2. IAEA C-1 quality assurance marble with zero specific activity of ^{14}C was used for the saturation scintillation absorption mixture. The MDA of the system was found to be 52.09 Bq/Kg C for a counting time of 200 minutes.

$$MDA\left(\frac{Bq}{Kg\ C}\right) = \frac{2.7 + 4.65 * \sqrt{B}}{\varepsilon \times m \times t} \quad [2]$$

Where, B is background counts of the system.

Active Sampling method

The Experimental setup for the active sampling method was shown in Figure 3. The system contains a pump (12V DC pump), flow controller, and two bubblers containing the Sodium hydroxide solution (NaOH). Atmosphere air was pulled through bubblers containing the 200 ml of 2N NaOH solutions.

Minimum Sampling period for the active sampling method

The minimum sampling period was determined based on the minimum amount of carbon required for the measurement of carbon-14. The minimum amount of carbon needed for measurements of ^{14}C using LSC with carbon dioxide absorption method was 0.95 g (approximately

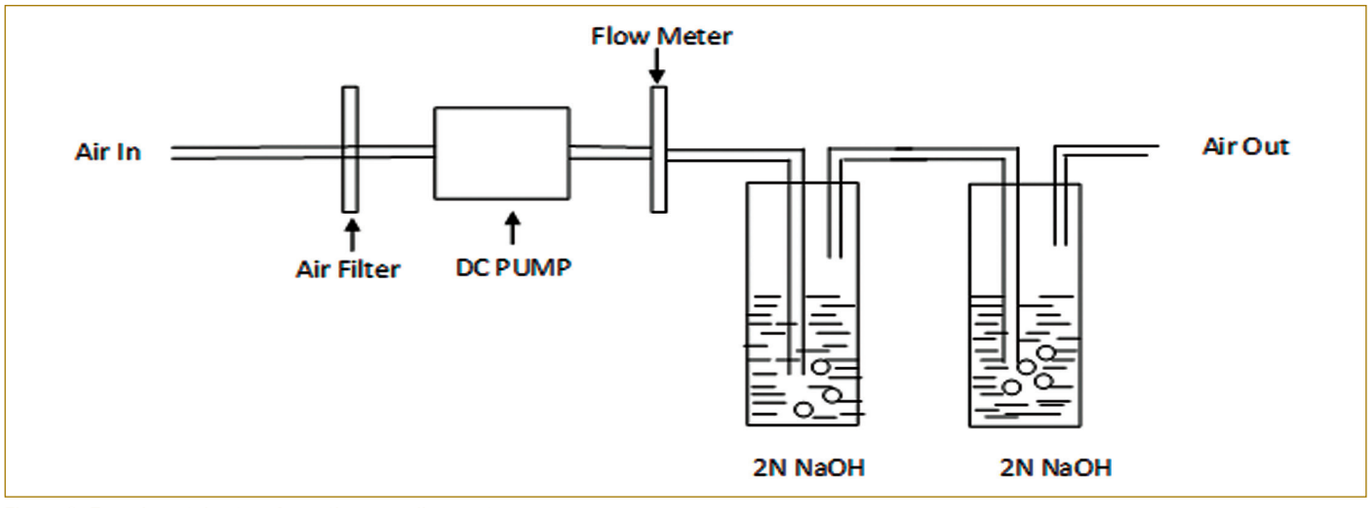

Figure 3: Experimental set up for active sampling system

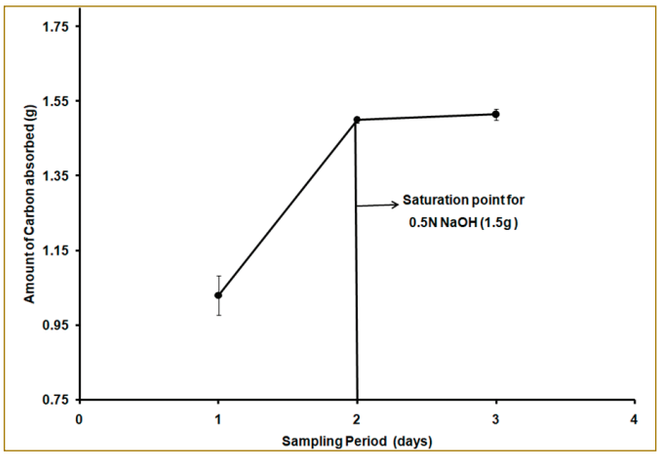

Figure 4: Mass of the carbon absorbed in 0.5N NaOH solution using PS

3.5 g of CO_2). The minimum sampling duration required for ^{14}C monitoring in the atmospheric air was calculated based on the following eq-3.

$$\text{Sampling duration (days)} = \frac{A}{B * C * D * 24 * 60} \quad [3]$$

A = Amount of CO_2 required (3.5 g)
B = Density of CO_2 (2 g/L)
C = Flow rate= 0.4 LPM
D = Concentration of CO_2 in the air (417 ppmv)

Calculation shows that a minimum of 7.5 days sampling period was required to collect 3.5 g of CO_2. Hence, the minimum sampling duration required for ^{14}C monitoring using the active sampling method was eight days.

Absorption of CO_2 in Sodium Hydroxide

Sampling was carried out with a flow rate of 0.4 LPM for eight days. After sampling, the amount of carbon trapped in the NaOH solution was measured using a TOC analyzer. Table 1 shows the mass of total carbon absorbed in each bubbler. The average amount of carbon absorbed was 1.071 ± 0.006 g. It was observed that an average of 91% of the total carbon was absorbed in the first bubbler, and the remaining 9% was absorbed in the second bubbler.

Table-1: Mass of the carbon trapped in active sampling technique

Sl.No	Sampled air volume (L)	Mass of the carbon absorbed (g)		
		Bubbler-1	Bubbler-2	Total
1	4608	0.980±0.009	0.101±0.007	1.081
2	4608	0.966±0.017	0.103±0.006	1.068
3	4608	0.976±0.011	0.087±0.017	1.063
4	4608	0.973±0.007	0.101±0.008	1.073
5	4608	0.965±0.010	0.105±0.015	1.070

Passive sampling method

Atmospheric CO_2 was collected directly by exposing the freshly prepared sodium hydroxide solution (500 mL) kept in a passive sampler to the atmosphere. A polyethylene rectangular tray of dimensions 30 cm x 15 cm x 6 cm (length x breadth x height) was used as a passive sampler (PS) in this study.

Sampling period for the passive sampling method

The amount of atmospheric CO_2 absorbed in 500 ml of 0.5N NaOH solution on different number of exposure days was studied. The saturation capacity of 500 ml of 0.5N NaOH solution is 1.5 g of carbon. All the sampling experiments were carried out in triplicates at the same location in an outdoor atmosphere with a mean temperature of 27 ± 6°C. Figure 4 shows the mass of the carbon trapped in PS at different sampling periods (days). It was observed from Figure 4 that 0.5N NaOH was saturated with atmospheric CO_2 for the sampling duration of two days. As discussed earlier, sampling will be terminated once the minimum mass of carbon needed for ^{14}C measurements using the CO_2 absorption method was absorbed. Hence, the minimum sampling period required for ^{14}C measurements in the atmosphere air was found to be one day using 500ml of 0.5N NaOH solution where the mass of carbon trapped was around 1g of carbon.

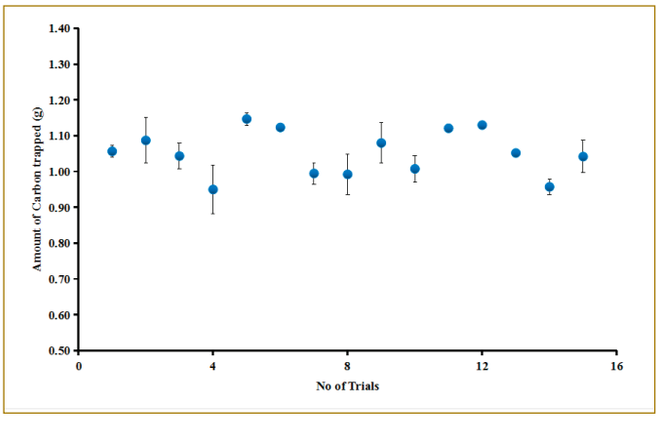

Figure 5: Mass of the carbon trapped in 0.5N NaOH solution using PS

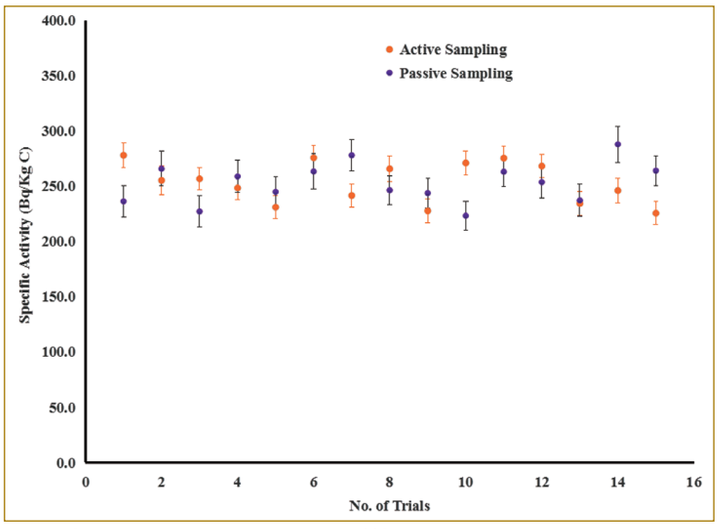

Figure-6: Measured specific activity of ^{14}C in the atmospheric air

Sampling of atmospheric $^{14}CO_2$ using passive samplers

The repeatability measurements of the absorption capacity of CO_2 from atmospheric air in 0.5 N NaOH solutions were carried out 15 times. 500 ml of 0.5N NaOH solutions were exposed for one day in the outdoor atmosphere within the IGCAR campus. The mass of the carbon absorbed in the passive sampler was measured using the TOC instrument and presented in Figure 5. The average mass of the carbon absorbed was found to be 1.05±0.06 g.

Recovery

Recovery experiments were mimicked to the recovery of carbonate formed in active and passive air sampling experiments. To the freshly prepared 500 ml of 0.5 N NaOH solutions, 1 g carbon equivalent of the analytical reagent grade anhydrous sodium carbonate (Na_2CO_3) was added. The carbonate present in the solution was precipitated as barium carbonate by the addition of barium chloride solution (22% w/v of $BaCl_2.2H_2O$) as per the stoichiometric balanced chemical reaction (a). The barium carbonate precipitate formed was separated by filtration method and dried. Recovery percentage values was calculated as per eq-4 and presented in Table 2. The average recovery percentage was found to be 98.67±0.29%.

Table.2.Recovery Studies for carbonate from CO_2 trapped in NaOH solution

Sodium Carbonate (g)	Theoretical weight of $BaCO_3$ (g)	Actual precipitate weight of $BaCO_3$ (g)	Recovery of carbonate (%)	Carbon in $BaCO_3$ (%)
8.8	16.38	16.15	98.58	6.06
8.79	16.36	16.20	99.00	6.02
8.89	16.55	16.29	98.43	6.03

Theoretical or Expected weight was determined based on the stoichiometric calculations from the weight of the sodium carbonate used in the study.

The carbon content in the barium carbonate precipitate obtained from the recovery process was analyzed using an elemental analyzer (CHNS). The theoretical carbon content per gram of barium carbonate is 6%. The measured percentage of carbon content in the precipitate was presented in Table 2, and it was found that the measured values of average carbon content in the precipitate were within the theoretical value of carbon content in the barium carbonate.

$$Recovery\ [\%] = \frac{weight\ of\ barium\ carbonate\ precipitate}{Theoretical\ or\ Expected\ weight} * 100 \quad [4]$$

Measurement of carbon-14

The $^{14}CO_2$ present in the precipitated $Ba^{14}CO_3$ was then subsequently absorbed into the CS/PE absorption mixture by acid hydrolysis and measured in the LSC to estimate ^{14}C activity. The measured specific activity levels of ^{14}C using active and passive sampling methods for 15 sampling trials were presented in Figure 6. The average ^{14}C specific activities were 253.4 ± 18.5 Bq/kg C and 252.8 ± 18.22 Bq/kg C, using active and passive sampling techniques, respectively. The measured specific activity levels of ^{14}C varied from 225.6 to 278.0 in the case of active sampling and where as 223.3 to 287.9 Bq/Kg C in the case of passive sampling method.

Conclusions

Sampling methodologies for the measurement of radiocarbon levels in the atmosphere was optimized with respect to sampling duration and absorption capacity of CO_2 in NaOH. The minimum sampling period required for ^{14}C monitoring in the atmosphere using NaOH solution was found to be one day in the case of passive sampling method where as eight days for active sampling method. The average measured ^{14}C specific activities were 253.4 ± 18.5 Bq/kg of C and 252.8 ± 18.22 Bq/kg of C, using active and passive sampling techniques, respectively. The passive sampling technique can be used for rapid sampling to assess the ^{14}C specific activity levels in the atmosphere in remote areas around the Nuclear Power Plants. The active sampling method is useful for routine monitoring of atmospheric ^{14}C concentrations.

Young Officer's Forum

Mr. Somnath Sengupta did his M.Sc in Chemistry from Indian Institute of Technology, Kharagpur and joined in Materials Chemistry & Metal Fuel Cycle Group, IGCAR as Scientific Officer-C after graduating from 13th batch of BARC Training School at IGCAR, Kalpakkam. Presently, he is working as Scientific Officer-D and his research areas include experimental and theoretical studies on the application of different extractants and Metal Organic Frameworks(MOFs) for the extraction of precious metals and actinides.

Highly Efficient Post-Synthetically Modified UiO-66 MOF for the Extraction of Pd(II) from Aqueous Solutions: Experimental and Theoretical studies

The advent of widespread globalization has lead to increase in consumption of platinum group metals (PGMs) due to their unique role in catalysis, pharmaceuticals, automobile industries, etc. Palladium is one of the PGMs that is in great demand and is used extensively in electronic and electrical equipment. It is also a key component of fuel cells, catalytic converters of the automotive industry, and anti-pollution devices. In addition, its role as a highly efficient industrial catalyst for countless chemical transformations is indispensable. Despite its high demand and large-scale consumption, availability of palladium in earth's crust is sparse (<10-6 %), due to which there is a need for alternative sources of palladium other than naturally occurring ores. In this context, nuclear industry provides a unique solution, where nuclear waste having a plethora of elements, can be used as an alternative source of palladium. Various porous materials like activated carbon, carbon nanotubes, graphite, graphene oxide, silica etc., have been widely employed for the recovery of palladium. However, these porous materials mostly displayed lower adsorption capacity. In this context, it is important to shift focus to another class of porous materials called metal organic frameworks (MOFs), which have demonstrated higher adsorption capacity. There have been various reports where MOFs have been used for the extraction of palladium from slightly acidic solutions with pH ranging from 2 to 6.

The extraction of palladium with the aid of MOFs shows higher adsorption capacity and kinetics as compared to other class of porous materials. Herein, we also focus on the extraction of Pd(II) from chloride medium, using zirconium based MOF, UiO-66-NH2, which is known for its high stability owing to the presence of strong Zr(IV)-carboxylate bonds. Due to the high surface area and porosity of these classes of MOFs, facile diffusion of ions/molecules occurs into the three-dimensional network thus enhancing the adsorption ability. Another advantage of using MOF is that appropriate functional groups can be incorporated in it, in order to tune its selectivity and adsorption efficiency. By adopting post-synthetic modification strategy, it is possible to modify the functional group in UiO-66-NH2, to make it more selective for specific metal ions. In this context, we have adopted PSM strategy to functionalize UiO-66-NH2 with two different ligands such as o-phenylenediamine and dithizone, which possess soft donor atoms like N and S, thereby increasing the affinity of the functionalized MOF for Pd(II) following HSAB principle. The synthesis was carried out using the strategy given in Figure 1. We used FTIR (Figure 2) and Powder XRD (Figure 3) to characterize the synthesized MOFs. EXAFS analysis at Zr K-edge was carried out to

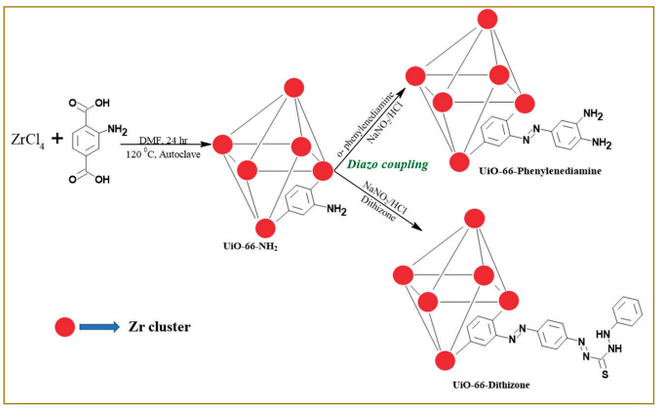

Figure 1. Synthetic strategy for the preparation of parent and PSM MOFs.

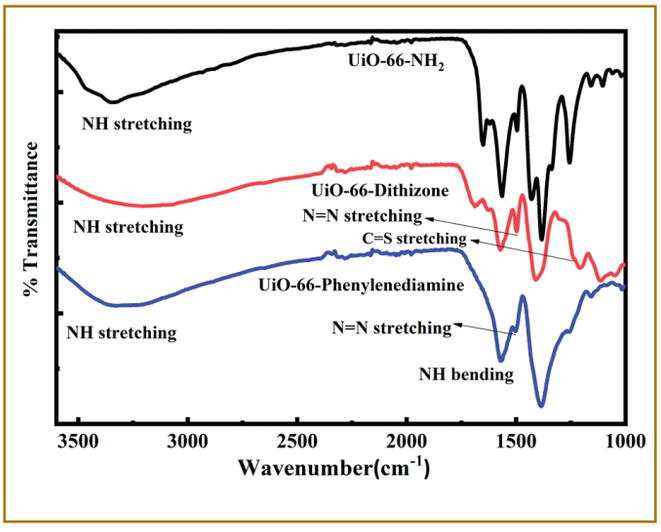

Figure 2 ATR-FTIR spectra of UiO-66-NH2, UiO-66-Dithizone and UiO-66-Phenylenediamine

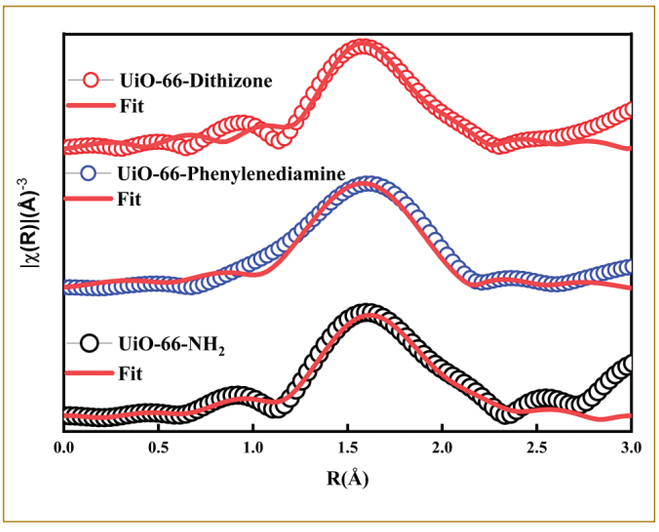

Figure 4 Extended region fitting at Zr-K edge using ARTEMIS in R-space.EXAFS data were fitted with k-weight of 3 from 2 to 10 Å^{-1}.

obtain explicit information about local environment of Zr in the synthesized parent and PSM MOFs. Theoretical computations were used to determine initial structural parameters for fitting EXAFS spectra. The best fits of the theoretical data with experimental one for all the three MOFs in R-space are given in Figure 4.

The EXAFS study gave insight into primary coordination sphere of Zr, where it was seen that Zr was coordinated to 8 oxygen atoms in parent UiO-66-NH2 MOF, with two oxygens at a distance of 2.14 Å, four oxygens at 2.28 Å and two oxygens at 2.31 Å. The bond distances and coordination sphere of the Zr subunit in the MOF UiO-66-NH2, closely match with the single crystal data of UiO-66-NH2.Comparison of EXAFS results of parent MOF with PSM MOFs revealed that there was a decrease in coordination number of Zr from 8 to 7 in case of both UiO-66-Phenylenediamine and UiO-66-Dithizone, which can be attributed to the formation of some defects at the octahedral Zr sites during post synthetic modification process.

Effect of solution pH on sorption of Pd(II)

The pH of solution plays a decisive role in the sorption behavior of a species on MOF. This may be ascribed to variables like variations in the metal ion's speciation with changing pH levels as well as changes in surface charge across MOF's binding sites due to protonation and deprotonation of the functional moieties. In Figure 5, relationship between sorption % of the parent and PSM MOFs and pH of palladium

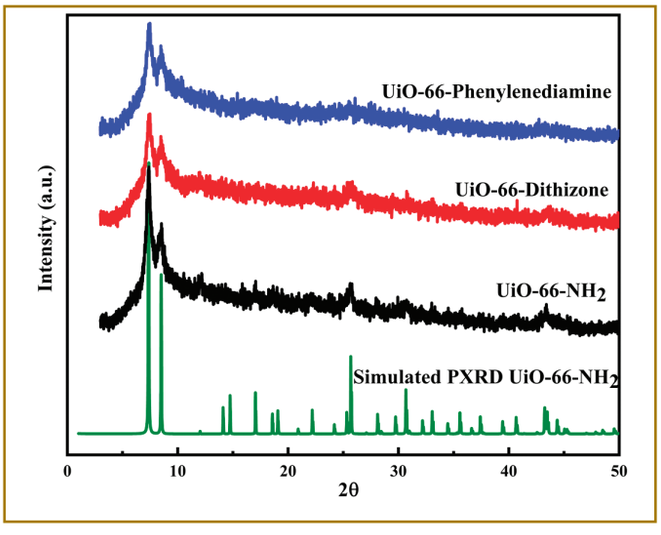

Figure 3 Powder-XRD patterns of UiO-66-NH2, UiO-66-Dithizone and UiO-66-Phenylenediamine

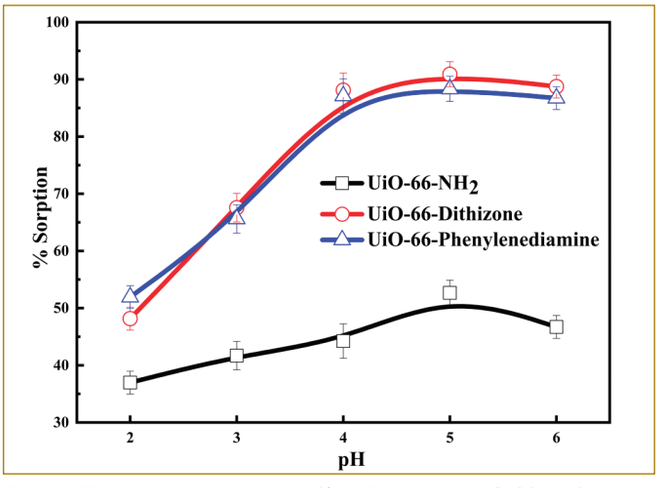

Figure 5 The variation in sorption (%) of Pd(II) onto UiO-66-NH2, UiO-66-Dithizone and UiO-66-Phenylenediamine with respect to pH; msorbent=10 mg, t=180 min, Vsolution= 3 mL, Co= 1000 mg L-1,T = 25ºC ±1

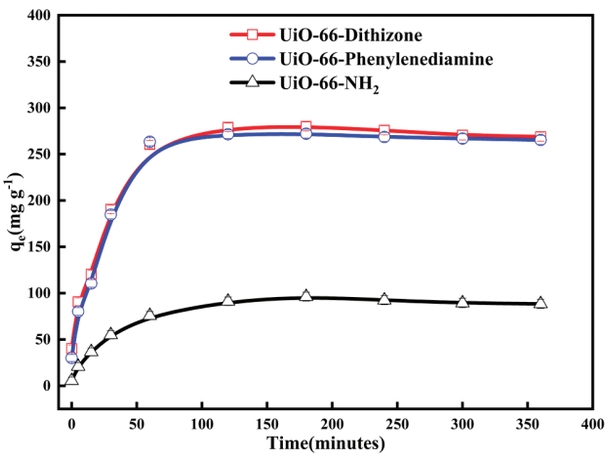

Figure 6 The effect of contact time on the amount of Pd(II)sorbed onto UiO-66-NH2, UiO-66-Dithizone and UiO-66-Phenylenediamine at pH 5;msorbent = 10 mg, t = 0 to 360 min, Vsolution= 3 mL, Co= 1000 mg L-1, T = 25°C±1.

solution is explained.

It was observed that with increase in pH of solution, percentage sorption increased for all three MOFs reaching a maximum at pH 5 after which decrease in sorption was observed. Percentage sorption for Pd(II) at pH 5 followed the order: UiO-66-Dithizone>UiO-66-Phenylenediamine>UiO-66-NH2. Sorption capacity (qe), distribution ratio (Kd) and sorption efficiency of all three MOFs at pH 5 is given in Table 1.

Table-1: Sorption of Pd(II) onto UiO-66-NH2, UiO-66-Dithizone and UiO-66-Phenylenediamineat pH 5

MOF	*qe*	*Kd*	% Sorption
UiO-66-NH_2	96±2.9	333±9	52±1.9
UiO-66-Dithizone	280±3.6	3001±41	90±2.3
UiO-66-Phenylenediamine	272±3.7	2274±33	88±2.3

Kinetics of sorption

The rate of sorption of Pd(II) on the three MOFs from aqueous solution was studied by varying the equilibration period from 0 min to 6 hours. The results revealed that there is an increase in sorption capacity till 3 hours after which it reaches almost saturation (Figure 6).

Kinetic study of sorption of Pd(II) revealed that UiO-66-NH2andthe PSM MOFs displayed a linear plot between contact time and t/qt. The plot was fitted into the linear form of pseudo-second order kinetic equation which is as follows:

$$\frac{t}{q_t} = \frac{t}{q_e} + \frac{1}{K_2 q_e^2},$$

where t is contact time, qt is sorption capacity(mg/g) of MOF at time t, K2 is the pseudo-second order rate constant and qe is the sorption capacity at equilibrium. The linear fit showed a correlation coefficient of greater than 0.98. K2 and qe obtained from the plot showed good agreement with experimental results as shown in Table 2. The kinetics of the sorption behavior suggests that sorption of Pd(II) on the MOFs is mainly controlled by chemical interactions operating between the MOF and Pd(II), rather than simple physical adsorption. So diffusion of Pd(II) plays an important role in deciding the rate of sorption. The swift increase in sorption capacity can be attributed to presence of a large magnitude of binding sites initially, after which there is a slight decrease in sorption which is owing to the saturation of binding sites leading to blockage of pores thereby hindering free diffusion.

Table-1: Kinetic Parameters for the Adsorption of Pd(II)on UiO-66-NH2, UiO-66-Dithizone and UiO-66-Phenylenediamine at pH 5

MOF	*qe (mg g-1)*	*K2 (g mg-1min-1)*	R^2
UiO-66-NH2	96±2.9	333±9	0.994
UiO-66-Dithizone	280±3.6	3001±41	0.997
UiO-66-Phenylenediamine	272±3.7	2274±33	0.997

Theoretical Studies

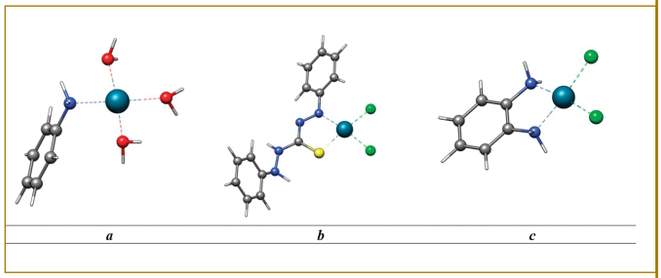

Figure 7. Optimized geometries of the lowest energy complexes for each ligand (a) Pd-aniline,(b) Pd-Dithizone (c) Pd-Phenylenediamine at BP86/def2-TZVP level. Color code: grey balls are carbon, blue balls are nitrogen, yellow balls are sulfur, dark cyan ball is palladium, and white colour represents hydrogen atoms.

Owing to high computational cost of modeling the entire metal-organic-framework (MOF) structure, we have adopted simplified binding ligands in our calculations that represent functional site of the MOFs. For instance, UiO-66-NH2, UiO-66-Phenylenediamine and UiO-66-Dithizone, were modelled in our calculations as aniline, o-phenylenediamine and dithizone, respectively. These ligands and complexes with Pd(II) were subjected to systematic geometry optimization at RI-BP86-D3BJ/def2-TZVP level in order to obtain the lowest energy structures, which were further characterized as energy minima by performing harmonic frequency analysis. The lowest energy structure for the complexes is shown in Figure 7. In order to quantify complexing ability of each ligand with Pd(II) was evaluated complexation energies for each metal complex by taking energy difference of reactants from products which shows negative values highlighting the favorable nature of the complexation process.

Young Researcher's Forum

Shri Choudhury Abinash Bhuyan acquired his M.Sc. in Physics from Utkal University, Odisha in 2018. He is currently a Senior Research Fellow (SRF) in the Surface and Sensors Studies Division, Materials Science Group, IGCAR. He specializes in the synthesis using chemical vapour deposition and localized characterization of monolayer di-chalcogenide films and device fabrications. Mr. Bhuyan has presented his work in Am. Phys. Soc. and many other international conferences. He is also a recipient of the prestigious K. V. Rao Sci. Soc. 'Best Researcher' award in 2023.

Large Area Monolayer MoS_2: Enhanced Optical and Electronic Properties

Recently, monolayer MoS_2 attracted a great deal of attention because of its exciting optoelectronic properties. One of the most exciting properties of MoS_2 is the transition of band gap from indirect to direct type as the thickness reduces from bulk to a monolayer. Besides, the quantum yield (QY) of the photoluminescence (PL) emission is enhanced by four orders as the thickness of MoS_2 is reduced to a monolayer, resulting in exploration for several optoelectronic applications such as photodetectors, transistors and solar cells. Even though MoS_2 is an excellent light absorber, it suffers from the low QY of the PL emission because of the off-stoichiometry of MoS_2 and the presence of structural defects.

Several methods were adopted to enhance the PL intensity of monolayer MoS_2, e.g., p-doping showing the maximum enhancement of ~9 times, passivation of S vacancies by the physisorption and chemisorption of molecules like O_2, H_2O and thiols. The chemisorption process depletes the electrons, enhancing the radiative recombination process and weakening the electrostatic screening of neutral excitons, which subsequently increases the PL intensity. A relative amount of ~150 times enhancement in PL intensity was reported in the chemisorption process. Laser irradiation of the monolayer MoS_2 was also found to be an efficient way of passivating the defects, leading to a 200-time increase in the PL intensity. In another approach, PL intensity of monolayer MoS_2 was increased up to ~160 folds using the plasmonics

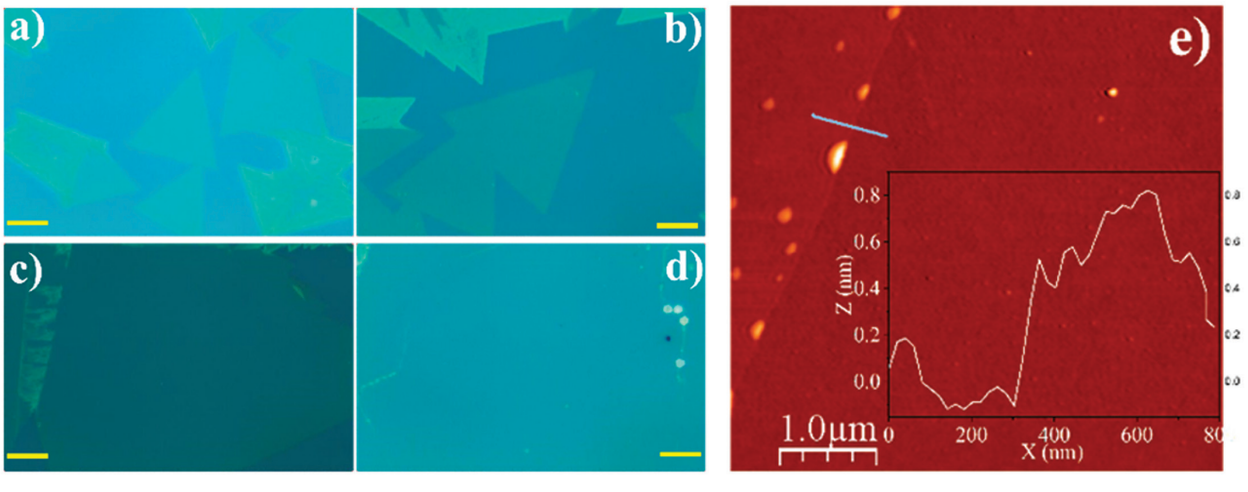

Figure : 1. (a,b) Optical micrographs of monolayer MoS_2 grown on SiO_2(300 nm)/Si. (c, d) A grain-free large-area monolayer. The scale shown is 10µm. (e) AFM topography image of monolayer MoS_2. The Inset image of the line profile reveals that the thickness of the MoS_2 layers is less than 0.9 nm.

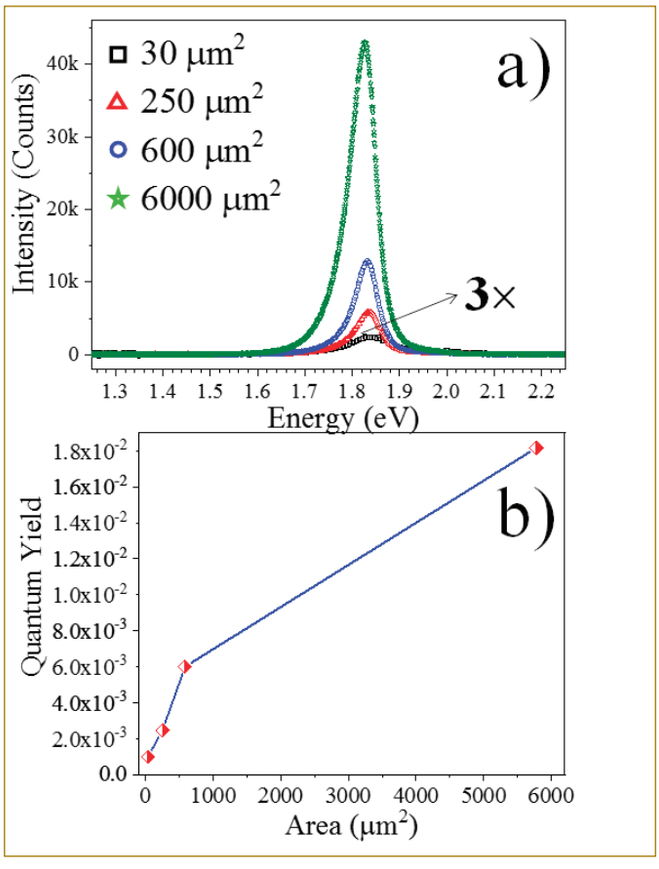

Figure : 2 (a) Typical PL spectra of MoS_2 monolayers collected from the different monolayer MoS_2 with varying area. (b) Variation of QY with the flake area of the monolayer sample.

materials and metasurfaces. Till now, the QY of monolayer MoS_2 is improved with the passivation of surface defects, suppressing the defect-mediated non-radiative recombination, which affects the inherent properties of monolayer MoS_2. Notably, the local temperature strongly influences the intensity and QY of PL emission. However, the effect of heat-dissipation in PL QY of monolayer MoS_2 was overlooked.

Monolayer MoS_2 samples were grown on SiO_2 (300 nm)/Si substrate using the atmospheric pressure chemical vapor deposition technique. Molybdenum trioxide (MoO_3, 99.97% Sigma Aldrich) and S (±99.5% pure; Sigma Aldrich) were used as the precursors for the formation of MoS_2 phase. The growth was carried out using a three-zone furnace and a 1-inch quartz tube used as a reaction chamber. Alumina boats containing the S powder (40 mg) and the MoO_3 powder (15 mg) were kept in two extreme zones. During the growth process, the two extreme zones were maintained at temperatures of 160 °C (S) and 700 °C (MoO_3). The middle zone was maintained at 200 °C. The reactor was evacuated to the base pressure of 1×10^{-3} mbar and the chamber was filled with ultra-high pure Ar at room temperature. A 50 sccm of Ar flow rate was maintained during the ramping as well as growth time of 20 min.

The growth of the MoS_2 layers was confirmed by the optical microscopic analysis showing triangular layered structures all over the substrate (Fig. 1a-d) with varying sizes, including a large-area growth with a grain area ~6000 μm². We measured the thickness of these layers using atomic force microscopy (AFM) to confirm the formation of the monolayer. The line profiles of the AFM topographic images (Fig. 1e) showed the thickness of these layers < 0.9 nm, confirming the formation of monolayer.

The effect of the flake area on the PL intensity was studied (Fig. 2a). The PL intensity of monolayer MoS_2 increased with increasing the flake area of the monolayer and ~50 increase was recorded for the large area (~ 6000 μm²) monolayer, than that for the small area ~ 30 μm²). In the present report, the observed PL intensity enhancement is very significant as compared to other surface-treated monolayer MoS_2. Fig. 2b shows the variation of QY with the area of the flake. The QY measurements were carried out using the Rhodamine 6G (R6G) molecules as standard. The QY measurements of monolayer MoS_2 were measured in a two-step process 1) measurement of QY of R6G thin film and subsequently 2) QY measurements of monolayer MoS_2 with respect to R6G thin film. The R6G thin film was prepared with the aqueous 0.3 mM R6G solution over the SiO_2(300 nm)/Si substrate. The QY of R6G thin film was estimated using the aqueous 0.3 mM R6G solution as the reference. The QY of R6G thin film was 0.151. Subsequently, the QY of monolayer MoS_2 was measured using the R6G thin film as a reference. The QY of monolayer MoS_2 is also found monotonously increased with the flake area of monolayer MoS_2 (Fig. 2b). The QY of large-area monolayer MoS_2 (1.82%) is increased by an order (~ 20 times) as compared to a small-area sample (0.098%), monolayer MoS_2. In comparison to the earlier reports, the QY of large area sample is one order higher for the mechanically exfoliated pristine monolayer MoS_2 sample and two orders more than as-grown CVD monolayer MoS_2 as well as surface treated monolayer MoS_2. The increased PL intensity with increased flake area is attributed to the efficient heat dissipation facilitated by the large area flakes as the QY of PL is dependent on the local temperature. In general, the PL QY reduces with increased temperature. In the

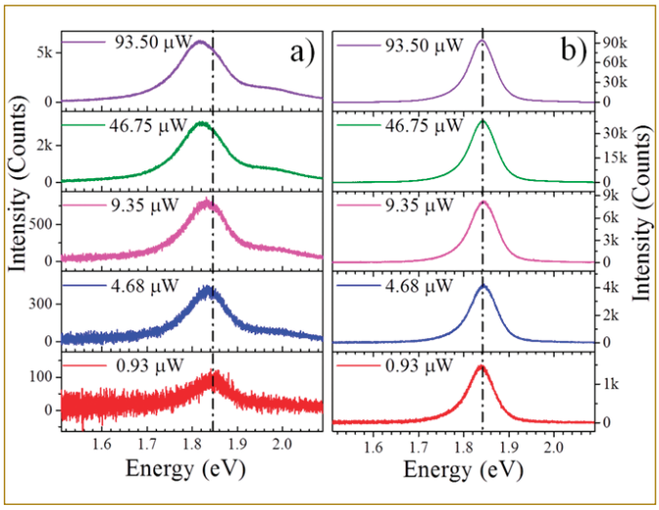

Fig. 3. Power-dependent PL spectra of a) small area (~30 μm²) and b) large area (~6000 μm²) MoS_2 flakes. Dash and dotted lines in the figures are guided to the eyes.

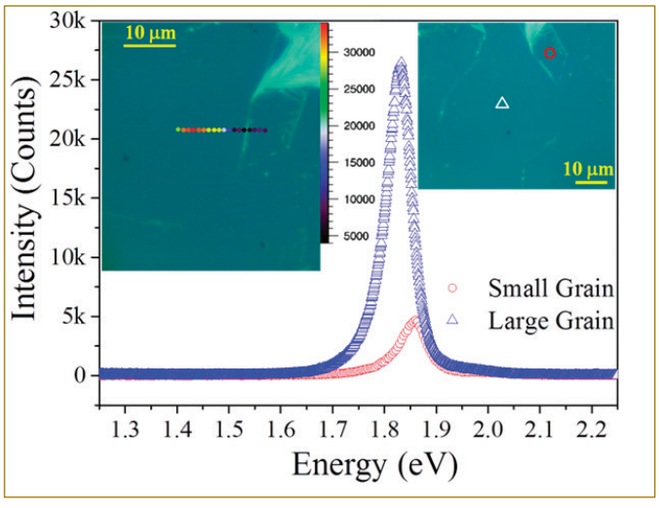

Fig. 4. Typical PL spectra of monolayer MoS_2 collected from the large (~2500 μm^2) and small (~135 μm^2) grains. The centres of the collected regions are indicated by an open triangle and circle in the optical micrograph, respectively (right hand side inset). PL line image is shown covering the part of the large and small grains (left side inset).

present case, the rise in the local temperature with laser-induced heat is minimal in large areas flakes due to efficient heat dissipation. Thus, PL intensity substantially increases in large-area flakes.

To ascertain our claim on the area-dependent increase of PL intensity, power-dependent PL measurements were carried out on small- and large-area monolayer MoS_2 flakes. In general, PL emission red-shifts with increasing laser power because of the heating effects. The PL emission was red-shifted with power in the case of a small-area flake (Fig. 3a). However, the large-area PL emission was negligibly shifted with laser power (Fig. 3b). Thus, it further confirms that the heating effect is more in a small-area flake, whereas the large- area flake is less affected because of availability of heat dissipating area.

In addition, the effect of the grain boundaries on heat dissipation was also explored. For this study, we have selected the region such that it comprises a large area and a small grain adjacent to it. The optical micrograph of such a region is shown in the inset of Fig. 4 (top right side). Fig. 4 shows the PL spectra collected from a large-area (~2500 μm^2) grain as well as a small-area (~135 μm^2) grain. In this case, PL intensity enhancement was also observed for large-area grain as compared to the small-area grain. The dependence of PL intensity on the grain size indicates that the grain boundaries are acting as a barrier for dissipation even though they represent a large-area growth. The PL imaging was carried out along the line, which covered the large grain region as well as the small grain region (inset of Fig. 4, left side). PL intensity is reduced near the boundary region and inside the small grain.

Monolayer devices fabricated with large channel dimensions may not meet the required demand to fabricate miniaturized and compact next-generation electronic devices. In other words, there is a trade-off between the availability of large heat-dissipating areas and the compactness of the devices. Therefore, it is imperative to eliminate the bottleneck by designing a compact structure that retains the characteristics of large-area monolayer MoS_2. It is worth mentioning that the optical absorption coefficient in the visible wavelength of the electromagnetic spectrum of monolayer samples is significantly high compared to that for conventional semiconductors. However, the overall light absorption is limited by the atomic scale thickness of monolayer MoS_2. Thus, the structure containing multiple layers possessing the monolayer behaviour will be necessary for a significant amount of absorbed light in the visible range. The PL properties of nanoscrolled monolayer MoS_2 vary significantly depending on the fabrication process. Till date, the nanoscrolls were mostly fabricated by the self-rolling method. The self-rolling was initiated by the evaporation of volatile organic solvent over the monolayer. Usually, isopropyl alcohol (IPA) and acetone were used as organic solvents because of their low surface tension and high evaporation rates. However, the PL emission studies were absent in nanoscrolls fabricated using IPA. In contrast, the self-rolled nanoscrolls fabricated with the aid of acetone showed four times higher PL intensity. The strain-induced MoS_2 nanoscrolls fabricated using ethanol solution (volume ratio of ethanol: water = 2:1) showed properties of multilayered MoS_2 with reduced PL QY.

We demonstrate an effective and facile route to fabricate the thermally stable nanoscrolled monolayer MoS_2. The self-rolled nanoscrolls were fabricated by using absolute ethanol. The room temperature PL spectra of monolayer MoS_2 and nanoscrolled monolayer MoS_2 are shown in (Fig. 5). The PL imaging was carried out using A-exciton intensity. The PL intensity was high over the scroll region compared to remnant MoS_2. The integrated PL intensity was increased by ~ 6 times compared to remnant monolayer MoS_2. The enhancement in the PL emission was attributed to negligible interlayer coupling among constituent layers.

The PL QY of monolayer film and nanoscrolled MoS_2 were calculated to be 1.3% and 2.95%, respectively. The QY of the nanoscrolled sample is 1.6 times higher than that measured for large-area monolayer film. The higher QY was attributed to the enhancement of PL emission in nanoscrolled MoS_2 compared to the planar form.

FET devices were fabricated on planar and nanoscrolled monolayer MoS_2 to evaluate the electrical properties. Both planar and nanoscrolled monolayer MoS_2-based back-gated FETs were fabricated with the same channel length of 10 μm. The fabrication protocols of FET are described step by step: 1) The electrodes were prepared by mask-less laser lithography technique via the lift-off method and contact metals were deposited by the thermal evaporator. The source and drain electrodes were fabricated with bimetals, Au (100 nm)/Ti (100), over the $MoS_2/SiO_2/Si$ flakes and scrolls. Subsequently, substrates with devices were thoroughly cleaned to remove the polymer residues, photoresist and other contaminants. 2) A universal bottom-gate electrode was prepared by Gallium-Indium eutectic as it formed an Ohmic contact with Si substrate. 3) The output and transfer characteristics for all FETs were measured by using a source measurement unit at room temperature. FESEM images of FET devices fabricated on planar and scrolled monolayer MoS_2 were shown in Fig. 6a and 6b, respectively.

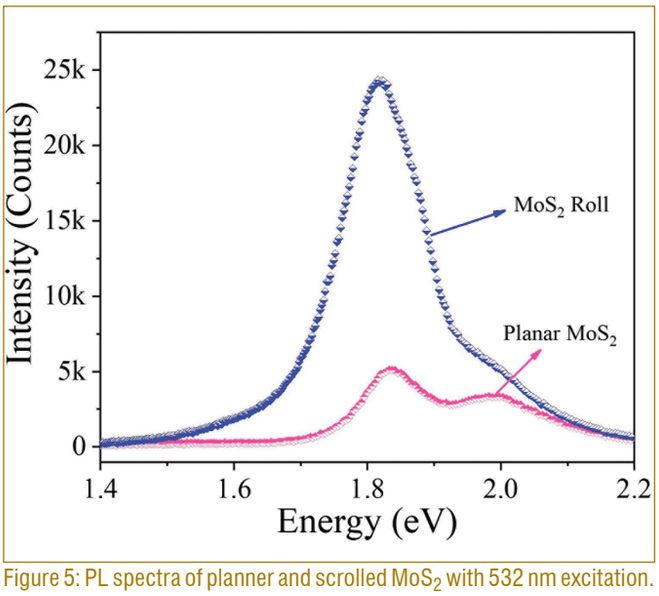

Figure 5: PL spectra of planner and scrolled MoS_2 with 532 nm excitation. The dotted line is the guides to the eyes.

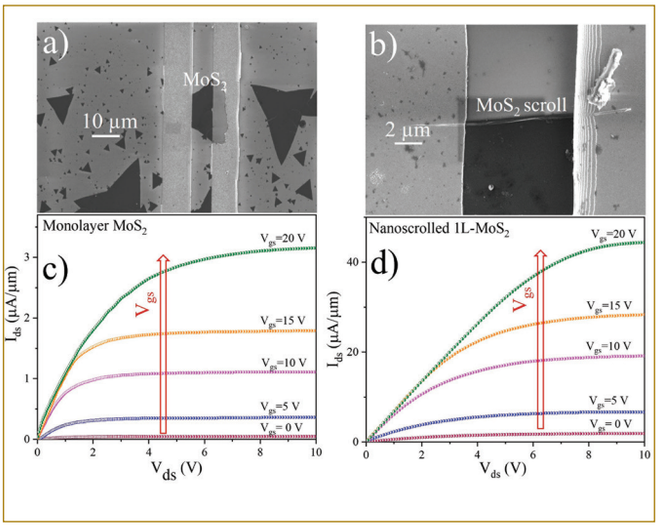

Figure 6: FESEM image of typical FET devices fabricated on planar (a) and scrolled monolayer MoS_2 (b) Output characteristics of (c) planar monolayer and (d) nanoscrolled monolayer MoS_2 FET.

In the output characteristics, the gate voltage (V_{gs}) was varied from 0 V to 20 V with an interval of 5 V (Fig. 6a and 6b). In both planar and nanoscrolled monolayer MoS_2-based FET devices, $_{I}$ds were found to raise linearly up to V_{ds} of ~4 V and thereafter saturated. The observed Ids versus V_{ds} results in both the devices are typical behaviour of FET devices. At V_{gs} of 20 V, the saturation drain currents are 3 and 45 μA/μm for planar and nanoscrolled monolayer MoS_2, respectively. The one-order (15 times) higher drain current is attributed to the availability of multiple paths for transporting the electrons in scrolled MoS_2 compared to planar monolayer MoS_2. For similar device configurations, the saturation drain currents reported in the literature are 1.35 and 0.14 μA/μm for planar MoS_2.

We extracted the threshold voltage, electron mobility and on/off current ratio from the transfer characteristics of both planar and scrolled MoS_2. The threshold voltage ($_{V}$t) was calculated using Y-function method. The mean V_t values are 5.7 and 5.2 V for planar and nanoscrolled MoS_2, respectively. Earlier, it was reported that V_t was substantially decreased by increasing the number of MoS_2 layers. However, the minute decrement in V_t for nanoscrolled MoS_2 is attributed to weak interlayer coupling that exists among the constituent layers of the scroll. Generally, the on-state performance of the FET is influenced by the carrier mobility.

The dimensions (L×W) of the planar and scrolled device are 10 × 10 μm^2 and 10 × 0.5 μm^2, respectively. The slope $\Delta I_{ds}/\Delta V_{gs}$ is calculated from the transfer characteristics curve in a linear regime at V_{ds} of 1 V. The field-effect electron mobility is calculated to be ~11 and ~2000 $cm^2V^{-1}s^{-1}$ for planar and nanoscrolled samples, respectively. The on/off current ratio for scrolled MoS_2 was 107 and the value was one order higher than that for the planar monolayer sample. The above results indicate that nanoscrolled monolayer MoS_2 exhibits superior electronic properties compared to planar monolayer MoS_2. Moreover, a one-order higher current ratio makes the scrolled MoS_2 suitable for digital applications.

In summarizing, we studied the effect of inherent properties of monolayer MoS_2, such as laser heating and heat-dissipation mechanism on the photoluminescence (PL) quantum yield (QY). The rise in the local temperature reduced as the area of the monolayer increased because of efficient heat dissipation. Consequently, the PL intensity increases with increasing the area of the monolayer. With efficient heat dissipation, the large-area monolayer shows the experimentally measured QY of 1.8%, which is higher by two orders for CVD-grown samples even after surface treatment. In further improving both the optical and device properties of monolayer MoS_2, we fabricated a compact device in the form of a nanoscroll. The PL QY (2.95%) of nanoscroll MoS_2 was significantly higher than the reported PL QY of untreated monolayer MoS_2. FET device fabricated on nanoscroll monolayer MoS_2 has shown one order higher on/off ratio and two order higher mobility compared to the device fabricated on planar monolayer MoS_2. Therefore, fabricated nanoscrolls can be used for compact and high-performance optoelectronic devices.

Technology Transfer of Penetration Enhancing Activated Flux for TIG welding of Stainless Steels

October 12, 2023

A penetration enhancing activated flux for TIG welding of stainless steel has been developed by Metallurgy & Materials Group (MMG) of IGCAR and has been patented in India, United Kingdom, USA and Ukraine. This flux increases weld penetration by as much as 12 mm in single pass welding and mitigate variable weld penetration in low sulphur containing steels. The technology was advertised in DAE websites in August'2023 as available to private sector for commercialisation through the technology transfer route. An industry based in Indore, specialising in welding technology, applied for technology transfer license to commercialise this technology. Accordingly, the technology

Transfer of MMG, IGCAR's "Penetration enhancing Activated Flux for TIG welding of Stainless Steels" to an Indore industry on 12.Oct.2023; Standing (L-R): Dr. N. Subramanian (Head, Incubation Centre, IGCAR), Dr. R. Divakar (Director, MMG), Licensee industry's partners and Dr. M. Vasudevan (Associate Director, MDTG, MMG); Left Inset: Presentation by licensee industry on their interest in this IGCAR technology; Right Inset: Photograph depicting the high welding penetrability in SS achieved with this patented IGCAR's technology

transfer was done during a brief event held at IGCAR on October 12,2023. Director, MMG handed over the technology transfer documents to the Indore industry in the presence of Associate Director (Materials Development & Technology Group), Head Incubation Centre-IGCAR and other Heads of Divisions/Sections of MMG.

Reported by
Dr. N. Subramanian
Head, Incubation Centre,
Safety, Quality & Resource Management Group

Two day Theme meeting on Fast Reactor Aerosol Research: Current Scenario and Future Directions (FARAR – 2023)

October 26-27, 2023

A theme meeting on FAST REACTOR AEROSOL RESEARCH - Current Scenario and Future Directions (FARAR-2023) was conducted at Indira Gandhi Centre for Atomic Research, Kalpakkam on 26th and 27th October 2023. The theme meeting was jointly organized by IGCAR and Safety Research Institute, SRI (AERB), in association with the Indian Association for Radiation Protection (IARP-K), Indian Society for Radiation Physics (ISRP-K) and Board of Research in Nuclear Sciences (BRNS). The theme meeting covered lectures on aerosol research from different perspectives such as, nuclear aerosol research relevant to Fast Reactors, environmental aerosols and bio-aerosols. The theme meeting also touched upon safety aspects of Sodium cooled Fast Reactors, which is very relevant in the current scenario where India is on the verge of commissioning the 500 MWe Prototype Fast Breeder Reactor.

Release of Souvenir by Shri. Sudhir B. Shelke, Station Director, MAPS during the inaugural function of theme meeting FARAR-2023

Panel discussion chaired by Dr. B. Venkatraman, Director, IGCAR

Shri Sudhir B. Shelke, Station Director, MAPS, inaugurated the theme meeting and addressed the gathering. A souvenir was released on the occasion. The inaugural address was followed by presidential address Dr. N. Sivaraman, Director, Chemistry Group and a special address by Dr. D. K. Mohapatra, Head of Division, Safety Research Institute. The theme meet had 5 sessions of invited lectures by eminent speakers from national research labs, academic institutions and also from DAE fraternity. Shri. K. V. Suresh Kumar, CMD, Bhavini, in his talk, highlighted India's flagship reactors, FBTR and PFBR, as he shared from his vast experience. Dr. B. K. Sapra and Dr. R. Baskaran elaborated about aerosol research in BARC and IGCAR respectively. Prof. Arul Prakash and Prof. Anupindi from the Indian Institute of Technology shed light on the state of the art computational tools and software available for modelling aerosol dynamics. After the technical sessions, there was a poster presentation session by researchers from IGCAR and ISRO. A panel discussion chaired by Dr B. Venkatraman, Director, IGCAR was organized in the afternoon of the second day of the program. The importance of collaborations between research institutes and academia and the need for further experimental and computational research was pointed out in the deliberations. The theme meeting provided the opportunity for experts from national laboratories to share their vast experience, provide insights and guide future direction in the field of aerosol research.

Reported by
Dr. A. Jasmin Sudha, ATBS / RESD
Safety, Quality & Resource Management Group

REcent ADvances in Information Technology (READIT – 2023)

November 22-23, 2023

Scientific Information Resource Division (SIRD), IGCAR in association with Madras Library Association - Kalpakkam Chapter (MALA- KC) organized the 13th Biennial International Conference on Recent Advances in Information Technology (READIT) during November 22-23, 2023 at Sarabhai Auditorium, IGCAR, Kalpakkam, with the theme 'Emerging Trends and Innovations in Libraries".

The conference was organized as an International event with participation from Sri Lanka and UAE. About two hundred delegates from the academic and public domain, Information Technology Professionals and Research scholars attended the conference.

In the inaugural function, Smt. S. Rajeswari, Convener READIT, AD, IRSG & Head SIRD delivered the welcome address. The function was presided over by Dr. N. Sivaraman, Outstanding Scientist, Director, MCMFCG, IGCAR. In his presidential address, Dr. N. Sivaraman highlighted the emerging technologies for libraries and the need for librarians in providing the required information to the scientists and engineers. Inaugural address was given by Dr. K. Nageswara Rao, Director, DESIDOC, New Delhi where he mentioned about digital asset management and preservation aspects. Dr. K. Nageswara Rao also Dr. S. A. V. Satyamurty, Director (Research), Vinayaka Mission Research Foundation and Former Director, IGCAR delivered the special address and released the Conference Proceedings. Shri E. Soundararajan, organising secretary READIT and Head DRTS, SIRD, IGCAR proposed the vote of thanks. Dr. S. A. V. Satyamurty inaugurated the exhibition stalls of publishers and vendors.

The conference included invited talks by domain experts in Information Science & Technology and oral presentations by Research Scholars & Professionals on both offline and online mode. The topics included evolving Information Resources Models and discovery tools, Open Science & Research data management, innovative technologies for future libraries, education policies and role of libraries and librarians in enabling scholarly communication. Special technical session was organised for the contributed presentations by Research Scholars and delegates which included oral presentations. The conference facilitated good interactions among young researchers, students, professionals and well-known speakers in the area of future technologies for libraries.

There was a specials session on 50 years of SIRD at the end of the day1. Dr. S. A. V. Satyamurty presided the SIRD 50 years function and released coffee table book on SIRD 50 years. Shri E. Soundararajan presented a brief journey about 50 years of SIRD achievements. Prof. M. Saibaba, Ramaiah University, bengaluru and former Director RMG, IGCAR delivered the special address. A specially crafted memento was presented to all the SIRD colleagues.

There was a panel discussion moderated by Smt. S. Rajeswari Prof. D. Arivudainambi, Director, Library Anna University, Prof.R.Sevukan, Pondicherry University, Shri. M Paul Pandian. Librarian IMSc, Shri. Manoj Singh, Head, IRMS, SIRD, BARC, Dr. V. Gopakumar, Digital University, Kerala and Prof. Jhon Philips, AD, MMG,IGCAR participated in the panel discussion on trends in scientific publication landscape.

The conference concluded with the valedictory function. Shri. E. Soundararajan delivered welcome address, Smt. S. Rajeswari presented the conference summary and Prof. K. Nithyanantham, President MALA gave special address. The valedictory address was given by Dr. N. Sivaraman. He has also presented the best paper awards of READIT 2023. Shri. P. Vijaya Gopal, Head, LIMS,SIRD,IGCAR proposed the vote of thanks.

Best Paper/Poster Award

- Dr. Amit Kumar, Ms. Usha Pujala, Shri E. Hemanth Rao, Dr. V. Subramanian, Shri. Sanjay Kumar Das, Dr. D. Ponraju, and Dr. B. Venkatraman secured the 'Best Platform Presentation' award at the Indian Aerosol Science and Technology Association (IASTA) National Conference 2023, held at Hotel Vivanta, Navi Mumbai, during 12 -14 December 2023 for the paper titled "Assessment of Fission Product and Sodium Aerosol Behavior in a closed chamber".

Bio-diversity @ DAE Campus, Kalpakkam

Lesser Goldenback are very common in both IGCAR campus and Kalpakkam township. It has a golden yellow and black upper plumage and black and white streaked lower parts and breast. Forehead differs in male and female, Female has a black forehead stippled with white and crimson hint crest. Mostly seen singly or in pairs.

Published by Safety, Quality & Resource Management Group, IGCAR, Kalpakkam-603102